Physics and Imaging in Radiation Oncology 9 (2019) 1–6

Contents lists available at ScienceDirect

Physics and Imaging in Radiation Oncology

journal homepage: www.elsevier.com/locate/phro

Original Research Article

Changes in apparent diffusion coefficient radiomics features during dose-painted radiotherapy and high dose rate brachytherapy for prostate cancer

Sangjune Laurence Lee[a,b], Jenny Lee[a,b], Tim Craig[a,b], Alejandro Berlin[a,b], Peter Chung[a,b], Cynthia Ménard[a,b,c], Warren D. Foltz[a,b,*]

[a] Radiation Medicine Program, Princess Margaret Cancer Centre, University Health Network, Toronto, Ontario, Canada
[b] Department of Radiation Oncology, University of Toronto, Toronto, Canada
[c] Centre de Recherche du Centre Hospitalier de l Université de Montréal (CRCHUM), Montréal, Canada

ARTICLE INFO

Keywords:
Diffusion-weighted MRI
Apparent diffusion coefficient
Radiomics
Prostate cancer
Dose-painted radiotherapy
High dose rate brachytherapy

ABSTRACT

Background and purpose: Dose escalation has improved cancer outcomes for patients with localized prostate cancer. Targeting subprostatic tumor regions for dose intensification may further improve outcomes. Apparent Diffusion Coefficient (ADC) maps may enable early radiation response assessment and dose adaptation. This study was a proof-of-principle investigation of early changes in ADC radiomics features for patients undergoing radiotherapy with dose escalation to the gross tumor volume (GTV).

Materials and methods: Fifty-nine patients were enrolled on a prospective tumor dose-escalation trial. Multi-parametric MRI was performed at baseline and week six, corresponding to the time of peak ADC change. GTV and prostate contours were deformably registered between baseline and week six T2-weighted images, and applied to ADC maps, to account for diminished image contrast post-EBRT and possible differences in prostate gland volume, shape, and orientation. A total of 101 radiomics features were tested for significant change post-EBRT using two-tailed Student's *t*-test. All ADC features of the prostate and GTV volumes were correlated using Pearson's coefficient ($p < 0.00008$, based on Bonferroni correction).

Results: ADC feature extraction was insensitive to $b = 0\ s/mm^2$ exclusion, and to gradient non-linearity bias. GTV presented predominant changes in first-order features, particularly 10Percentile, and prostate volumes presented predominant changes in second-order features. Changes in both first and second-order features of GTV and prostate ROIs were strongly correlated.

Conclusions: Our data confirmed significant changes in numerous GTV and prostate features assessed from ADC and T2-weighted images during radiotherapy; all of which may be potential biomarkers of early radiation response.

1. Introduction

Despite technical improvements to external beam radiation therapy (EBRT), 15–30% of patients with intermediate to high risk localized prostate cancer develop disease recurrence [1]. Targeting subprostatic regions of higher tumor burden for dose intensification to an imaging defined gross tumor volume (GTV) could improve tumor control probability and reduce dose to organs-at-risk [2].

PIRADS version-2 (v-2) criteria provide standardized diagnostic guidelines for GTV identification and scoring from MR images [3], primarily based on signal features in T2-weighted (T2w) images and apparent diffusion coefficient (ADC) maps derived from diffusion-weighted images (DWI). Compared to PIRADS v-2 criteria, radiomics applied to multi-parametric MR images can improve the automated detection, localization, and grading of prostate tumor [4–6]. Applied to radiotherapy, radiomics analysis of pretreatment multi-parametric MR images can predict for biochemical recurrence [7], and rectal wall toxicity [8], and have been used to generate focal treatment plans when combined with MRI-to-CT deformable co-registration [9].

Radiomics may also improve on current use of first-order ADC metrics as early radiation response biomarkers which may then guide dose adaptation [10,11]. Response assessment has historically tracked changes in mean GTV ADC post-EBRT, based on a consensus position that prostate tumor ADC is inversely related to tumor cellularity

* Corresponding author at: Department of Radiation Oncology, Princess Margaret Cancer Centre, University Health Network, 101 College Street, 7th Floor, Toronto, Ontario M5G 1L7, Canada.
E-mail address: Warren.Foltz@rmp.uhn.ca (W.D. Foltz).

https://doi.org/10.1016/j.phro.2018.11.006
Received 12 May 2018; Received in revised form 16 November 2018; Accepted 19 November 2018
2405-6316/ © 2018 The Authors. Published by Elsevier B.V. on behalf of European Society of Radiotherapy & Oncology. This is an open access article under the CC BY-NC-ND license (http://creativecommons.org/licenses/BY-NC-ND/4.0/).

[12–14]. Our own data identified week six as the time of peak change in prostate tumor ADC [11]. This study also noted a trend towards homogenization of ADC across the tumor and zonal regions post-EBRT, which may be reflected in textural features and variance metrics in whole prostate regions-of-interest. Potentially, whole prostate radiomics metrics could provide a surrogate of GTV response, without need for computationally-intensive deformable registration in post-EBRT cases when the GTV is no longer apparent.

This study is a proof-of-principle investigation of early changes in ADC radiomics features for patients undergoing radiotherapy. Methodology is presented to assess prostate gland and gross tumor volume (GTV) features in PIRADS v-2 compliant T2-weighted images and ADC maps between baseline and week six. This methodology includes deformable registration between time-points of T2-weighted image sets and GTVs applied to ADC maps, to account for image contrast homogenization post-EBRT. Features presenting significant differences post-EBRT were extracted, plus prostate and GTV features were correlated to test for inter-predictive value.

2. Materials and methods

Between November 2012 and August 2016, patients with localized prostate cancer were enrolled on an institutionally-approved prospective tumor dose-escalation trial, based on either simultaneous integrated boost (SIB) or high dose rate brachytherapy boost (HDRB) at the discretion of the patient and their treating physician. All patients received 76 Gy in 38 fractions delivered to the prostate gland using volume modulated arc therapy (VMAT). SIB arm patients received an additional 19 Gy to the GTV. HDRB arm patients received 10 Gy in a single fraction to the GTV the week prior to EBRT initiation.

2.1. MRI protocol

Image-guided confirmatory biopsy and fiducial marker placement was performed at baseline prior to EBRT, and follow-up scanning was performed during week six of EBRT. MR images were acquired using a 3T Verio (Siemens Medical Systems, Erlangen, DE) with VQ gradients (40 mT/m peak amplitude; 200 T/m/s peak slew rate), with a four-channel phased-array surface coil placed anterior to the pelvis in combination with a two channel endorectal coil (Hologic Inc. Bedford, MA). Pulse sequence details are provided as Supplementary Material.

2.2. Gradient non-linearity bias

The superior/inferior (S/I) offset of the central slice through the dominant lesion from MRI system isocenter was tracked at each time-point, because ADC bias from gradient non-linearity approaches 5% at 9 cm S/I offsets from isocenter [15]. Across all patients, the absolute offset of the central slice through the dominant tumor from magnet isocenter was 35 ± 28 mm at baseline (136 mm max), and 31 ± 24 mm at week six (83 mm max). The mean and standard deviation difference in slice offset between time-points was 33 ± 23 mm (93 mm max).

Three patients presented with absolute offsets of nine cm or greater at baseline or week six, which is an offset consistent with 5% ADC bias. The slice offset differences between time-points for these patients were 29, 52, and 68 mm. Exclusion of these three patients had minimal effect on the sets of extracted radiomics features.

2.3. Image analysis

ADC maps with and without b = 0 s/mm^2 DWI were analyzed because not all scanners and platforms can generate PIRADS v-2 compliant ADC maps with lowest b-value of 50–100 s/mm^2, and because features which are consistently significant may be more robust response metrics. The ADC maps including b = 0 s/mm^2 were derived in-line, and the PIRADS v-2 compliant ADC maps excluding b = 0 s/mm^2 diffusion-weighted images were derived using Matlab (Mathworks, Natick, MA), via weighted least squares regression to: $\mathrm{Log}(S(b)/S(b_{min})) = -(b - b_{min})^* ADC + c$, where b_{min} denotes the lowest b-value used for the regression and c is an arbitrary baseline. Weightings were proportional to the inverse of the signal variance. ADC accuracy and signal-to-noise adequacy for this protocol at b = 1000 s/mm^2 has been confirmed [16].

2.4. Tumor identification

Tumors were identified according to PIRADS v-2 parameters on treatment planning system (Pinnacle). Delineation was performed manually by expert radiation oncologists (CM, PC) to encompass all suspicious voxels on multiparametric MRI. In cases with multiple lesions, boost was applied to all lesions.

2.5. Deformable registration

Deformable registration between baseline and week six image sets and segmented volumes was performed to increase robustness to possible intra-scan motion, variations in prostate gland volume, shape, and orientation between imaging time-points [17,18], and loss of intra-prostatic image contrast post-EBRT [11]. Prostate boundaries and at least three common points were contoured on baseline and week six T2-weighted images, using MIPAV software (NIH, Bethesda, MD). The points provided an initial rigid alignment, and MORFEUS [19], a biomechanical-based deformable registration technique, computed displacement from baseline to the week six T2w GTV guided by the prostate surface. The deformable registration accuracy was measured by target registration signed error (TRE), calculated from the displacements between the observed and the MORFEUS-predicted point coordinates.

GTVs were drawn on baseline T2-weighted images, guided by characteristic tumor hypointensity in pre-treatment ADC maps, and then deformably registered to week six T2-weighted images. The baseline and week six GTVs were then applied to their corresponding ADC maps using MIPAV, and manually corrected as deemed necessary between ADC and T2-weighted images, to account for routine ADC distortion and inter-acquisition motion [13]. The extent of manual correction was quantified by calculation of the shift in Centre-of-Mass of each GTV using MIPAV.

Fig. 1 presents representative T2-weighted images, ADC maps, and GTV at each time point. Across all sets, TRE was calculated from 185 points corresponding to fiducial markers and/or natural landmarks. The average and standard deviation TRE was 0.7 ± 3.8 mm, 0.2 ± 2.9 mm, and 0.1 ± 6.9 mm in the LR, AP and SI directions respectively. The average magnitude of error vector was 4 ± 7 mm. Manual corrections of GTVs applied to ADC images from T2-weighted images were performed in 35 GTVs at baseline, and in 35 GTVs at week six. The mean and standard deviation vector shifts in GTV centres-of-mass were 2.3 ± 1.6 mm. Twenty vector shifts were greater than 3 mm, and eleven vector shifts were greater than 4 mm. In some cases, these GTV shifts were corrections from partially outside of the prostate gland or between zonal regions.

2.6. Radiomics feature extraction

Radiomics analysis used the open-source pyradiomics package [20], customized for feature extraction from GTV and prostate ROIs applied to baseline and week six ADC maps, and corresponding T2-weighted images. A total 101 radiomics features were extracted, which comprised the available pyradiomics feature set, excluding general image-specifying features which were not meaningful for signal characterization (e.g. BoundingBox, EnabledImageTypes; GeneralSettings; ImageHash; ImageSpacing; MaskHash; Version).

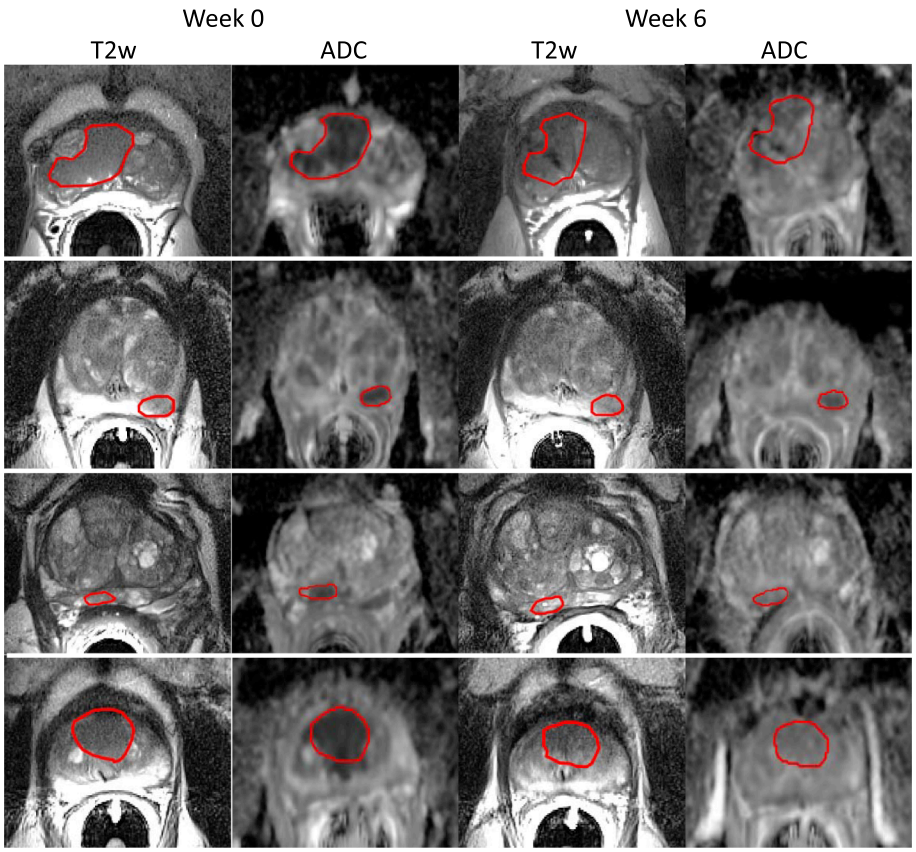

Fig. 1. T2-weighted images and ADC maps from four patients at baseline (left) and week six (right). These images emphasize the need for deformable registration, because of loss of prostate-to-tumor contrast post-EBRT and shifts in prostate orientation between time-points. Routine distortion in diffusion-weighted images compared to T2-weighted images motivates additional correction of GTVs applied to ADC maps.

2.7. Statistical analysis

Feature values were compared using two-tailed Student's *t*-test in Matlab, first between SIB and HDRB cohorts at baseline and week 6, and then between baseline and week 6 time-points using the pooled SIB and HDRB patient cohort. Correlations between the prostate and GTV feature values at baseline, week six, and their difference, were investigated using Pearson's correlation coefficient. These correlations were performed as part of a hierarchical clustering analysis (clustergram function, Matlab). In total, each feature was compared 603 times, comprised of two t-tests between SIB versus HDRB cohort values at baseline and at week 6; one *t*-test between baseline and week 6 for the pooled cohort values changes; and 600 comparisons from the hierarchical clustering analysis. For example, each baseline GTV ADC feature was correlated with 100 baseline, week six, and difference features for both ADC and T2w image sets. The corresponding p-value for significance is 0.00008 based on Bonferroni correction.

Prostate versus prostate, and GTV versus GTV feature correlations were not calculated because of highly similar contoured volumes. B = 0 s/mm^2-excluded ADC maps were not considered for prostate versus GTV feature comparison, because prostate ROIs copied from T2-weighted images sometimes encompassed low signal-to-noise regions within which ADC values were set to zero by the custom fitting algorithm.

3. Results

Patient characteristics for each arm are summarized in Table 1. Seventy-seven tumors were identified across the cohort of 59 patients. Single tumors were identified in 45 patients, and 32 tumors were identified in fourteen patients. A single patient was processed with four GTVs, two patients were processed with three GTVs, and eleven patients were processed with two GTVs.

Table 1
Summary of patient characteristics. Age and tumor volume are presented as mean ± 2 standard deviations.

	SIB	HDRB
No. of patients	29	30
Age (years)	70 ± 7	68 ± 6
Tumor vol. (cm^3)	2.2 ± 2.0	2.1 ± 1.4
Gleason score		
3 + 3	2	2
3 + 4	18	21
4 + 3	8	4
4 + 4	1	3
T Stage		
1c	10	12
2a	15	11
2b	1	3
2c	0	3
3a	3	1
PSA (ng/ml)		
≤10	24	20
> 10	5	10

3.1. Feature extraction from T2-weighted images

No significant differences in baseline or week six T2-weighted features were noted between SIB and HDRB arms. No features changed for GTVs applied to T2-weighted images, including tumor volumes (baseline: 2.2 ± 3.7 cm^3; week six: 1.9 ± 3.1 cm^3; p = 0.23). Seven features in T2-weighted images changed in whole prostate ROIs applied to T2-weighted images, of which only a reduction in the sphericity feature from 0.79 ± 0.05 to 0.72 ± 0.11 was highly significant.

Table 2
Most significantly different radiomics features for GTV ADC (mean ± 2σ). Bold-face denotes $p < 1e^{-07}$. The symbols * and ** denote units of 10^{-6} mm^2/s and $(10^{-6}$ mm^2/s$)^2$. The remaining features are dimensionless.

b = 0 s/mm^2 included			b = 0 s/mm^2 excluded		
Feature	Baseline	Week Six	Feature	Baseline	Week Six
10Percentile*	**825 ± 360**	**1100 ± 323**	**10Percentile***	**760 ± 459**	**1077 ± 392**
DifferenceEntropy	**3.99 ± 0.57**	**3.58 ± 0.63**	**SizeZoneNonUniformityNormalized**	**0.47 ± 0.14**	**0.39 ± 0.13**
Mean*	**1132 ± 387**	**1334 ± 265**	**SmallAreaEmphasis**	**0.71 ± 0.10**	**0.65 ± 0.12**
DifferenceVariance	**36 ± 38**	**18 ± 17**	**InterquartileRange**	**358 ± 223**	**253 ± 152**
MeanAbsoluteDeviation*	**202 ± 93**	**150 ± 78**	Median*	1077 ± 542	1312 ± 359
Median*	**1110 ± 426**	**1325 ± 271**	Mean*	1096 ± 501	1316 ± 346
RobustMeanAbsoluteDeviation*	**144 ± 75**	**104 ± 59**	InverseVariance	0.17 ± 0.09	0.22 ± 0.09
DifferenceAverage	**6.8 ± 3.6**	**5.0 ± 2.4**	MeanAbsoluteDeviation*	213 ± 132	157 ± 88
Interquartile Range*	**347 ± 190**	**248 ± 150**	Difference Average	7.1 ± 4.7	5.2 ± 2.7
RootMeanSquared*	**1161 ± 381**	**1349 ± 259**	RobustMeanAbsoluteDeviation*	153 ± 128	106 ± 61
SmallAreaEmphasis	**0.71 ± 0.10**	**0.65 ± 0.12**	RootMeanSquared*	1131 ± 499	1333 ± 340
GrayLevelVariance	**106 ± 91**	**63 ± 59**	GrayLevelVariance	123 ± 93	83 ± 84
Variance**	**66044 ± 57219**	**38861 ± 36831**	GrayLevelVariance	122 ± 143	74 ± 85
Contrast	**91 ± 102**	**47 ± 45**	SmallDependenceEmphasis	0.45 ± 0.21	0.38 ± 0.15
GrayLevelVariance	**106 ± 91**	**63 ± 59**	GrayLevelNonUniformityNormalized	0.03 ± 0.02	0.04 ± 0.03
SizeZoneNonUniformityNormalized	**100 ± 95**	**57 ± 55**	DifferenceEntropy	3.9 ± 1.2	3.6 ± 0.7
SumSquares	**3.9 ± 1.2**	**3.6 ± 0.7**	RunEntropy	5.4 ± 0.8	5.1 ± 0.8
Entropy	**5.2 ± 0.6**	**4.8 ± 0.8**			
ClusterTendency	5.2 ± 0.6	4.8 ± 0.8			
Ld	0.26 ± 0.08	0.21 ± 0.09			
InverseVariance	0.18 ± 0.07	0.22 ± 0.09			
GrayLevelVariance	112 ± 86	75 ± 67			
GrayLevelNonUniformityNormalized	0.03 ± 0.01	0.04 ± 0.03			
RunEntropy	5.4 ± 0.6	5.1 ± 0.8			
Uniformity	0.03 ± 0.02	0.04 ± 0.03			

3.2. Feature extraction from GTV ADC

No significant differences in baseline or week six ADC features were noted between SIB and HDRB arms. With SIB and HDRB arms pooled, significant GTV ADC feature changes between baseline and week six are presented in Table 2. GTV ROIs presented with significant changes in 32 and 17 features for ADC without and with b = 0 s/mm^2 exclusion, but the number of highly significant features (bold-face in Table 2) reduced from 17 to four with b = 0 s/mm^2 exclusion. The primary effect of b = 0 s/mm^2 exclusion appeared to be a decrease in absolute ADC metrics, and an increase in ADC variance metrics.

3.3. Feature extraction from prostate ADC

Prostate ROIs presented with changes in 40 and 19 features for ADC without and with b = 0 s/mm^2 exclusion. Eighteen of a maximum nineteen significantly different ADC features were common between b-value sets. The predominant prostate ADC feature changes between baseline and week six are presented in Table 3.

3.4. Prostate/GTV feature correlations

A large number of correlations between GTV and prostate features in T2-weighted images and ADC maps at baseline and week 6 time-points are summarized in Table 4. The twenty strongest of the correlations between ADC feature changes in GTV and prostate volumes post-EBRT are summarized in Table 5, with dominant representation from first-order statistics (e.g. median and 90Percentile for prostate; 10Percentile and Mean for GTV) and textural features from the Gray Level Size Zone Matrix class (e.g. Zone Variance for Prostate; Low Gray Level Zone Emphasis for GTV). The corresponding clustergram is presented in Supplementary Material.

4. Discussion

Methodology was presented for assessing early changes in GTV and prostate radiomics features of ADC maps and T2w images for prostate cancer patients treated with radical radiotherapy. Deformable registration enabled propagation of GTV and prostate volumes from baseline and week six, when intra-prostatic image contrast is reduced and prostate shape, orientation, and volume may differ. A manual correction of the GTVs applied to ADC maps was then applied as deemed necessary to compensate for routine distortion in diffusion-weighted single-shot echo-planar images [16], and inter-scan motion. Radiomics analysis then identified a large set of GTV and prostate features which demonstrated early changes that may inform outcomes.

Numerous changes in ADC features in prostate and GTV volumes were presented. The prostate ADC histogram showed non-significant changes to the percentile histogram features, but standard deviation metrics reduced. Consistently, our prior results presented no significant change in the prostate ADC mean [11]. The ADC histograms of the GTV presented with a dominant increase in the 10Percentile feature, smaller increase in ADC mean, and equivalent high-percentile features. These results are consistent with consensus position that prostate tumor ADC is related inversely to cellular density [12–14]. The GTV also presented with reduced deviation/variances during treatment, as reported by features including homogeneity, entropy, and contrast. Our prior data also demonstrated that the effect of EBRT is a trend towards homogenization of zonal and tumor mean ADC values [11]. This finding is fully consistent with the identification of predominant variance and textural feature changes within the prostate gland post-EBRT (Tables 3 and 5).

Of interest is the value of zone-naïve prostate features instead of GTV features for assessment of treatment response, because a prostate-focused analysis would allow for stream-lined work-flow without need for time- and computationally-intensive deformable registration. Deformable registration may be required for a GTV-focused analysis given poorly visible prostate in post-EBRT MR images, as per the examples in Fig. 1. Out of the numerous correlating features noted in Table 4, of particular interest were the 61 correlations between ADC feature changes in GTV and prostate volumes. ADC is a broadly accepted biomarker of tumor response post-EBRT, unlike T2 which changes predominantly in the peripheral zone rather than in the central gland or GTV [11]. A very large number of correlations were also noted

Table 3
Most significantly different radiomics features for prostate ADC (mean ± 2σ). Bold-face denotes $p < 1e^{-07}$. The symbol * denotes units of 10^{-6} mm^2/s. The remaining features are dimensionless.

b = 0 s/mm^2 included			b = 0 s/mm^2 excluded		
Feature	Baseline	Week Six	Feature	Baseline	Week Six
RunLengthNonUniformityNormalized	**0.89 ± 0.02**	**0.87 ± 0.02**	**DependenceNonUniformityNormalized**	**0.23 ± 0.04**	**0.20 ± 0.03**
ShortRunEmphasis	**0.96 ± 0.01**	**0.95 ± 0.01**	**SizeZoneNonUniformityNormalized**	**0.41 ± 0.05**	**0.38 ± 0.04**
DifferenceAverage	**6.4 ± 1.5**	**5.4 ± 1.2**	**DifferenceAverage**	**6.8 ± 2.0**	**5.7 ± 1.4**
ZonePercentage	**0.44 ± 0.08**	**0.38 ± 0.08**	**SmallAreaEmphasis**	**0.67 ± 0.04**	**0.64 ± 0.04**
Ld	**0.26 ± 0.03**	**0.29 ± 0.04**	**InverseVariance**	**0.17 ± 0.05**	**0.20 ± 0.04**
RunPercentage	**0.94 ± 0.01**	**0.93 ± 0.02**	**LargeAreaHighGrayLevelEmphasis**	**53208 ± 39878**	**94978 ± 105575**
DifferenceEntropy	**4.0 ± 0.3**	**3.8 ± 0.3**	**ZonePercentage**	**0.44 ± 0.12**	**0.39 ± 0.08**
Ldm	**0.17 ± 0.03**	**0.20 ± 0.04**	SmallDependenceEmphasis	0.38 ± 0.10	0.33 ± 0.06
SmallDependenceEmphasis	**0.37 ± 0.06**	**0.33 ± 0.07**	Contrast	104 ± 90	71 ± 45
InverseVariance	**0.18 ± 0.03**	**0.21 ± 0.04**	SmallDependenceGrayLevelEmphasis	1390 ± 681	1106 ± 551
DependenceNonUniformityNormalized	**0.22 ± 0.03**	**0.20 ± 0.03**	RobustMeanAbsoluteDeviation*	171 ± 82	138 ± 62
LargeDependenceEmphasis	**9.0 ± 2.4**	**10.9 ± 3.2**	MeanAbsoluteDeviation*	258 ± 117	211 ± 94
LongRunEmphasis	**1.22 ± 0.05**	**1.26 ± 0.07**	GrayLevelNonUniformityNormalized	0.023 ± 0.009	0.03 ± 0.01
Contrast	**79 ± 41**	**56 ± 26**	DifferenceEntropy	4.1 ± 0.6	3.9 ± 0.3
RunVariance	**0.08 ± 0.02**	**0.10 ± 0.03**	RunEntropy	6.0 ± 0.5	5.8 ± 0.5
JointEnergy	**0.0013 ± 0.0008**	**0.0018 ± 0.0009**	GrayLevelVariance	188 ± 157	132 ± 120
SmallAreaEmphasis	**0.66 ± 0.04**	**0.63 ± 0.04**	InterquartileRange*	402 ± 224	328 ± 145
DependenceVariance	**2.2 ± 0.7**	**2.7 ± 0.9**	Maximum*	2986 ± 702	2733 ± 598
JointEntropy	**10.3 ± 0.8**	**9.8 ± 0.8**	SumSquares	183 ± 172	126 ± 123
LargeAreaEmphasis	**18 ± 14**	**33 ± 31**			
SizeZoneNonUniformityNormalized	**0.40 ± 0.04**	**0.37 ± 0.05**			
DifferenceVariance	**34 ± 20**	**24 ± 12**			
MaximumProbability	**0.003 ± 0.002**	**0.005 ± 0.003**			
ZoneVariance	**13 ± 13**	**26 ± 29**			
Uniformity	**0.025 ± 0.009**	**0.03 ± 0.01**			

Table 4
Numbers of correlated features within prostate and GTV volumes at baseline (BL) and week 6 (Wk 6). Δ refers to the feature change between time-points.

		Prostate, ADC			Prostate, T2w		
		BL	Wk 6	Δ	BL	Wk 6	Δ
GTV, ADC	BL	81	0	11	0	2	0
	Wk 6	14	9	8	0	0	0
	Δ	4	3	61	7	0	1
GTV, T2w	BL	0	0	26	1515	1	1
	Wk 6	0	0	40	0	307	14
	Δ	0	1	303	41	25	1762

between T2-weighted features and feature changes in the prostate and GTV. This result is consistent with similar T2 reduction post-EBRT for GTV and whole prostate [11].

Strengths of this study include implementation of standardizable approaches for radiomics, deformable registration, and ADC analyses. Feature extraction utilized the open-source Pyradiomics package and an appropriate Bonferroni correction. ADC accuracy of the Siemens Verio MRI system used in this study has already been validated, using the ice water standardization phantom [16,21]. ADC map generation included b = 0 s/mm^2 exclusion for PIRADS-2 compliance [4], but strong consistency was demonstrated between the extracted feature sets with and without b = 0 s/mm^2 exclusion for both GTV and prostate ROIs. The potential for gradient non-linearity bias was assessed by tracking the offset from isocenter of the dominant lesion [15]. Just three patients were found to be susceptible to gradient non-linearity bias, and repeated analyses with these patients excluded found minimal impact on the extracted feature sets.

The primary study limitation was the absence of analyses with regards to clinical outcomes. Instead, methodology for prostate ADC radiomics analysis was established, and promising early response features were identified. When mature outcomes become available, machine learning and radiogenomics methods are envisaged to test the predictive values of all features and their combinations [22,23]. A predictive algorithm which is robust and less reliant on post-EBRT GTV contours may be favored. It is hoped that a set of the dominant features noted in Tables 2, 3, and 5 will prove to be clinically relevant predictors.

Table 5
Twenty strongest correlations between GTV ADC and prostate ADC feature changes between baseline and week six of radiotherapy. Pearson's correlation coefficient (rho) for a p-value threshold of 0.00008 is approximately 0.50 for the cohort size of 59 patients. The rho value for these strongest correlations ranges from 0.54 to 0.60.

Prostate feature	GTV feature
ZoneVariance	LowGrayLevelZoneEmphasis
Median	10Percentile
ZoneVariance	ShortRunLowGrayLevelEmphasis
RootMeanSquared	10Percentile
ZoneVariance	LowGrayLevelEmphasis
VoxelNum	VoxelNum
Mean	10Percentile
ZoneVariance	SmallAreaLowGrayLevelEmphasis
ZoneVariance	SmallDependenceLowGrayLevelEmphasis
LargeDependenceEmphasis	LowGrayLevelZoneEmphasis
ZoneVariance	LowGrayLevelZoneEmphasis
90Percentile	Mean
VoxelNum	RunLengthNonUniformity
90Percentile	RootMeanSquared
DependenceVariance	LowGrayLevelZoneEmphasis
RootMeanSquared	Mean
LargeDependenceEmphasis	ShortRunLowGrayLevelEmphasis
DependenceVariance	ShortRunLowGrayLevelEmphasis
LargeDependenceEmphasis	LowGrayLevelRunEmphasis
DependenceVariance	LowGrayLevelRunEmphasis

This study also did not investigate quantitative T_2 mapping or DCE, though DCE images were used for tumor detection. T_2 shortening between malignant versus benign prostate and post-EBRT is known, but clinical T_2 mapping is superceded by T2-weighted imaging [11,24]. Quantitative DCE-MRI poses multiple standardization challenges [25], and its inclusion with T2w and ADC may not be necessary for more accurate radiomics-based prostate cancer diagnosis or staging [26].

To conclude, our preliminary data confirmed GTV and prostate radiomic feature changes in ADC and T2-weighted images during radiotherapy. These features warrant further investigation as potential predictive biomarkers of clinical outcomes.

Conflicts of interest

Dr. Chung reports personal fees from AbbVie, personal fees from Bayer, grants from Sanofit, outside the submitted work.

Dr. Craig reports grants from Canadian Cancer Society, grants from RaySearch Laboratories AB, during the conduct of the study.

Acknowledgements

This research was supported by grant funding from the Canadian Cancer Society.

Appendix A. Supplementary data

Supplementary data to this article can be found online at https://doi.org/10.1016/j.phro.2018.11.006.

References

[1] Spratt DE, Pei X, Yamada J, Kollmeier MA, Cox B, Zelefsky MJ. Long-term survival and toxicity in patients treated with high-dose intensity modulated radiation therapy for localized prostate cancer. Int J Radiat Oncol 2013;85:686–92. https://doi.org/10.1016/j.ijrobp.2012.05.023.

[2] Pollack A, Zagars GK, Smith LG, Lee JJ, von Eschenbach AC, Antolak JA, et al. Preliminary results of a randomized radiotherapy dose-escalation study comparing 70 Gy With 78 Gy for prostate cancer. J Clin Oncol 2000;18:3904–11. https://doi.org/10.1200/JCO.2000.18.23.3904.

[3] Purysko AS, Rosenkrantz AB, Barentsz JO, Weinreb JC, Macura KJ. PI-RADS version 2: a pictorial update. RadioGraphics 2016;36:1354–72. https://doi.org/10.1148/rg.2016150234.

[4] Khalvati F, Wong A, Haider MA. Automated prostate cancer detection via comprehensive multi-parametric magnetic resonance imaging texture feature models. BMC Med Imaging 2015;15:27. https://doi.org/10.1186/s12880-015-0069-9.

[5] Wang J, Wu CJ, Bao ML, Zhang J, Wang XN, Zhang YD. Machine learning-based analysis of MR radiomics can help to improve the diagnostic performance of PI-RADS v2 in clinically relevant prostate cancer. Eur Radiol 2017;27:4082–90. https://doi.org/10.1007/s00330-017-4800-5.

[6] Chaddad A, Kucharczyk MJ, Niazi T. Multimodal radiomic features for the predicting gleason score of prostate cancer. Cancers (Basel) 2018;10:E249. https://doi.org/10.3390/cancers10080249.

[7] Gnep K, Fargeas A, Gutiérrez-Carvajal RE, Commandeur F, Mathieu R, Ospina JD, et al. Haralick textural features on T2-weighted MRI are associated with biochemical recurrence following radiotherapy for peripheral zone prostate cancer. J Magn Reson Imaging 2017;45:103–17. https://doi.org/10.1002/jmri.25335.

[8] Abdollahi H, Mahdavi SR, Mofid B, Bakshandeh M, Razzaghdoust A, Saadipoor A, et al. Rectal wall MRI radiomics in prostate cancer patients: prediction of and correlation with early rectal toxicity. Int J Radiat Biol. 2018;94:829–37. https://doi.org/10.1080/09553002.2018.1492756.

[9] Shiradkar R, Podder TK, Algohary A, Viswanath S, Ellis RJ, Madabhushi A. Radiomics based targeted radiotherapy planning (Rad-TRaP): a computational framework for prostate cancer treatment planning with MRI. Radiat Oncol. 2016;11:148. https://doi.org/10.1186/s13014-016-0718-3.

[10] Song I, Kim CK, Park BK, Park W. Assessment of response to radiotherapy for prostate cancer: value of diffusion-weighted MRI at 3 T. Am J Roentgenol 2010;194:W477–82. https://doi.org/10.2214/AJR.09.3557.

[11] Foltz WD, Wu A, Chung P, Catton C, Bayley A, Milosevic M, et al. Changes in apparent diffusion coefficient and T2 relaxation during radiotherapy for prostate cancer. J Magn Reson Imaging 2013;37:909–16. https://doi.org/10.1002/jmri.23885.

[12] Padhani AR, Liu G, Koh DM, Chenevert TL, Theony HC, Takahara T, et al. Diffusion-weighted magnetic resonance imaging as a cancer biomarker: consensus and recommendations. Neoplasia 2009;11:102–25.

[13] Zelhof B, Pickles M, Liney G, Gipps P, Rodrigues G, Kraus S, et al. Correlation of diffusion-weighted magnetic resonance data with cellularity in prostate cancer. BJU Int 2009;103:883–8. https://doi.org/10.1111/j.1464-410X.2008.08130.x.

[14] Gibbs P, Liney GP, Pickles MD, Zelhof B, Rodrigues G, et al. Correlation of ADC and T2 measurements with cell density in prostate cancer at 3.0 Tesla. Invest Radiol 2009;44:572–6. https://doi.org/10.1097/RLI.0b013e3181b4c10e.

[15] Malyarenko D, Newitt D, Wilmes LJ, Tudorica A, Helmer KG, Arlinghaus LR, et al. Demonstration of non-linearity bias in the measurement of the apparent diffusion coefficient in multicenter trials. Magn Reson Med 2016;75:1312–23. https://doi.org/10.1002/mrm.25754.

[16] Foltz WD, Porter DA, Simeonov A, Aleong A, Jaffray D, Chung P, et al. Readout-segmented echo-planar diffusion-weighted imaging improves geometric performance for image-guided radiation therapy of pelvic tumors. Radiother Oncol 2015;117:525–31. https://doi.org/10.1016/j.radonc.2015.07.046.

[17] Nakazawa T, Tateoka K, Saito Y, Yano M, Yaegashi Y, Narimatsu H, et al. Analysis of prostate deformation during a course of radation therapy for prostate cancer. PLoS One 2015;10:e0131822https://doi.org/10.1371/journal.pone.0131822.

[18] Roach 3rd M, Faillace-Akazawa P, Malfatti C. Prostate volumes and organ movement defined by serial computerized tomographic scans during three-dimensional conformal radiotherapy. Radiat Oncol Investig 1999;5:187–94. https://doi.org/10.1002/(SICI)1520-6823(1997) 5:4<187::AID-ROI4>3.0.CO;2-U.

[19] Brock KK, Nichol AM, Ménard C, Moseley JL, Warde PR, Catton CN, et al. Accuracy and sensitivity of finite element model-based deformable registration of the prostate. Med Phys 2008;35:4019–25. https://doi.org/10.1118/1.2965263.

[20] van Griethuysen JJM, Fedorov A, Parmar C, Hosny A, Aucoin N, Narayan V, et al. Computational radiomics system to decode the radiographic phenotype. Cancer Res 2017;77:e104–7. https://doi.org/10.1158/0008-5472.CAN-17-0339.

[21] Malyrenko D, Galbán CJ, Londy FJ, Meyer CR, Johnson TD, Rehemtulla A, et al. Multi-system repeatability and reproducibility of apparent diffusion coefficient measurement using an ice-water phantom. J Magn Reson Imaging 2013;37:1238–46. https://doi.org/10.1002/jmri.23825.

[22] Stoyanova R, Takhar M, Tschudi Y, Ford JC, Solórzano G, Erho N, et al. Prostate cancer radiomics and the promise of radiogenomics. Transl Cancer Res. 2016;5:432–47. https://doi.org/10.21037/tcr.2016.06.20.

[23] Roebuck JR, Haker SJ, Mitsouras D, Rybicki FJ, Tempany CM, Mulkern RV. Carr-Purcell-Meiboom-Gill imaging of prostate cancer: quantitative T2 values for cancer discrimination. Magn Reson Imaging 2009;27:497–502. https://doi.org/10.1016/j.mri.2008.08.001.

[24] Heye T, Davenport MS, Horvath JJ, Feuerlein S, Breault SR, Bashir MR, et al. Reproducibility of dynamic contrast-enhanced MR imaging. Part 1. Perfusion characteristics in the female pelvis by using multiple computer-aided diagnosis perfusion analysis solutions. Radiology 2013;266:801–11. https://doi.org/10.1148/radiol.12120278.

[25] Kuess P, Andrzejewski P, Nilsson D, Georg P, Knoth J, Susani M, et al. Association between pathology and texture features of multi parametric MRI of the prostate. Phys Med Biol 2017;62:7833. https://doi.org/10.1088/1361-6560/aa884d.